nature structural & molecular biology

Structure of a kinesin–tubulin complex and implications for kinesin motility

Benoît Gigant[1], Weiyi Wang[2,4], Birgit Dreier[3], Qiyang Jiang[2,4], Ludovic Pecqueur[1,4], Andreas Plückthun[3], Chunguang Wang[2] & Marcel Knossow[1]

The typical function of kinesins is to transport cargo along microtubules. Binding of ATP to microtubule-attached motile kinesins leads to cargo displacement. To better understand the nature of the conformational changes that lead to the power stroke that moves a kinesin's load along a microtubule, we determined the X-ray structure of human kinesin-1 bound to αβ-tubulin. The structure defines the mechanism of microtubule-stimulated ATP hydrolysis, which releases the kinesin motor domain from microtubules. It also reveals the structural linkages that connect the ATP nucleotide to the kinesin neck linker, a 15–amino acid segment C terminal to the catalytic core of the motor domain, to result in the power stroke. ATP binding to the microtubule-bound kinesin favors neck-linker docking. This biases the attachment of kinesin's second head in the direction of the movement, thus initiating each of the steps taken.

Kinesins are microtubule-based molecular motors that use the energy derived from ATP hydrolysis to produce work. The conversion of chemical to mechanical energy is effected by a conserved motor domain that binds ATP and microtubules. Kinesins have roles ranging from intracellular transport to cell division, with most of the kinesins walking along microtubules to carry loads[1,2]; they have been grouped into 14 classes, on the basis of phylogenetic analysis of their motor domain[3]. Extensive biochemical studies have established that most motile kinesins move their load one 8-nm step per ATP hydrolyzed and that the power stroke (the ensemble of structural changes that cause movement) is distributed over one or several stages of the stepping cycle, including ATP binding to microtubule-bound kinesin[4,5].

To determine the structural changes that lead to movement production by kinesins, a high-resolution analysis is required. X-ray structures of kinesin motor domains are known[6], but the comparison of cryo-EM reconstructions of motile kinesins bound to microtubules with X-ray structures of unbound motor domains[7–9] demonstrates that this domain substantially changes its structure upon microtubule binding. Consistently, binding of kinesins to microtubules or tubulin changes the properties of the motor domain, in particular increasing the ATP hydrolysis rate by several orders of magnitude[10]. As a consequence, the X-ray structures of unbound motor domains do not provide direct information on the kinesin mechanism. The only structural information available on kinesin–microtubule complexes originates from cryo-EM, with the best resolutions being in the 10-Å range[7–9].

Because of the limited resolution of cryo-EM structural data, open questions remain about the kinesin mechanism. One question concerns how ATP binding to microtubule-bound motile kinesins leads to movement. In recent years, the view has emerged that in kinesins that move toward the plus end of microtubules, ATP binding to the nucleotide site controls the orientation of the neck linker, a 14–18 amino acid sequence C terminal to the catalytic core of the motor domain[5,9]. In a kinesin dimer, this biases the partner head toward the microtubule plus end[5]. In class 1 kinesin (kinesin-1, previously named 'conventional kinesin' and one of the most extensively characterized motile kinesins), the neck linker of the free kinesin is in equilibrium between a disordered state and a docked state[11], but it is docked in microtubule-bound kinesin–ATP[5]. However, the connection between ATP binding and neck-linker docking is unclear. The atomic structure of an ATP-loaded functional kinesin motor domain bound to a microtubule or to tubulin could provide information on this connection and, more generally, on the structural changes that lead to movement.

A second question relates to the mechanism for ATP hydrolysis by microtubule-bound motile kinesins. As translational motility occurs, ATP hydrolysis is required for a kinesin head in a dimer to detach from the bound tubulin and reach its new binding site. Slow ATPase activity of microtubule-bound kinesins would limit the rate of movement. Indeed, this process is considerably accelerated by microtubules. A high-resolution structure of a tubulin-bound kinesin would provide information on the underlying mechanism.

[1]Laboratoire d'Enzymologie et Biochimie Structurales, Centre de Recherche de Gif, Centre National de la Recherche Scientifique, Gif sur Yvette, France. [2]Institute of Protein Research, Tongji University, Shanghai, China. [3]Department of Biochemistry, University of Zurich, Zurich, Switzerland. [4]Present addresses: Laboratoire d'Enzymologie et Biochimie Structurales, Centre de Recherche de Gif, Centre National de la Recherche Scientifique, Gif sur Yvette, France (W.W.), Grenoble Outstation, European Molecular Biology Laboratory, Grenoble, France (Q.J.) and Laboratoire de Chimie des Processus Biologiques, Collège de France, Paris, France (L.P.). Correspondence should be addressed to C.W. (chunguangwang@tongji.edu.cn) or M.K. (knossow@lebs.cnrs-gif.fr).

Received 21 January; accepted 3 June; published online 21 July 2013; doi:10.1038/nsmb.2624

To define the structural changes in kinesin–ATP that lead to movement production, we determined the 3.2-Å-resolution structure of a monomeric kinesin-1 construct bound to an ATP analog, in complex with tubulin. In this structure, tubulin was curved, whereas it is straight in microtubules. We showed that changes in the tubulin-kinesin interface were limited upon the curved-to-straight transition of tubulin, providing a basis for the use of our structure in analysis of the mechanism of this motile kinesin. Our results revealed the relationship between the nucleotide state of the kinesin and the conformation of the neck linker. They also elucidated the mechanism for microtubule-stimulated kinesin ATPase.

RESULTS

Structure of a motile kinesin in complex with tubulin

Kinesin-1 is a dimer of identical kinesin heavy chains that both recruit a light chain. Its motor domain comprises a catalytic core and a 40-residue adjacent neck region[12]. Monomeric kinesin truncation products that comprise most of the motor domain (that is, the catalytic core and the ~15–amino acid proximal part of the neck region, named the neck linker) are sufficient to generate motility[5,13]. In agreement with previous results[14], our observed interactions of a functional monomeric kinesin-1 construct[5] with the αβ-tubulin heterodimer and with microtubules shared many features: the kinesin had similar affinities for both tubulin forms (**Supplementary Table 1**), and its ATPase activity was enhanced by more than two orders of magnitude by both microtubules and tubulin (**Table 1**).

We determined the structure of this kinesin construct bound to tubulin (**Fig. 1** and **Table 2**). Tubulin was further complexed with a designed ankyrin repeat protein (DARPin) that prevents tubulin self-assembly. The DARPin did not appreciably modify the interaction of the kinesin with tubulin, as the kinesin ATPase activities stimulated by tubulin or by the tubulin–DARPin complex were similar, with nearly identical catalytic constants and similar K_m (**Table 1**). In the crystals, the kinesin-bound nucleotide was a stable ATP analog, AMP-PNP, or an ATP-hydrolysis transition-state analog, ADP–AlF_4^-. Because both structures were similar, the analysis presented refers to the higher-resolution data, obtained with ADP–AlF_4^- (**Supplementary Fig. 1**). The kinesin bound both tubulin subunits of the same heterodimer (**Fig. 1a**), as had been inferred from electron micrographs of kinesin-decorated microtubules[15]. The kinesin-tubulin interface was composed of two interaction zones (**Fig. 1a**). One of them (**Fig. 1b,c**) was contributed to by α-tubulin. It involved residues in the short helices (H) H3′ and H11′ and in the N-terminal two turns of H12 as well as in the H11′–H12 loop; on the kinesin side, residues of loop (L) L11 as well as those on the tubulin-facing side of H4 and H6 were involved. The other interaction zone was mostly contributed to by β-tubulin H12, by

Table 1 Stimulation of the kinesin-1 monomeric construct ATPase by tubulin and microtubules

	Microtubules	Tubulin	Tubulin–DARPin
k_{cat} (s^{-1})	50.3 ± 1.6	16.1 ± 0.4	17.1 ± 0.6
K_m (μM)[a]	1.3 ± 0.1	9.7 ± 0.6	6.9 ± 0.6
Basal activity (s^{-1})		~0.1	

[a]The catalytic parameter that differs most between ATPase stimulation by tubulin and microtubules is the K_m, with values within a factor of <8 from each other, thus suggesting that the affinities of some of the kinesin species along the ATPase pathway differ. The affinities of monomeric kinesin for tubulin and microtubules differ more when ADP is bound than in the other nucleotide states where they were measured (**Supplementary Table 1**).

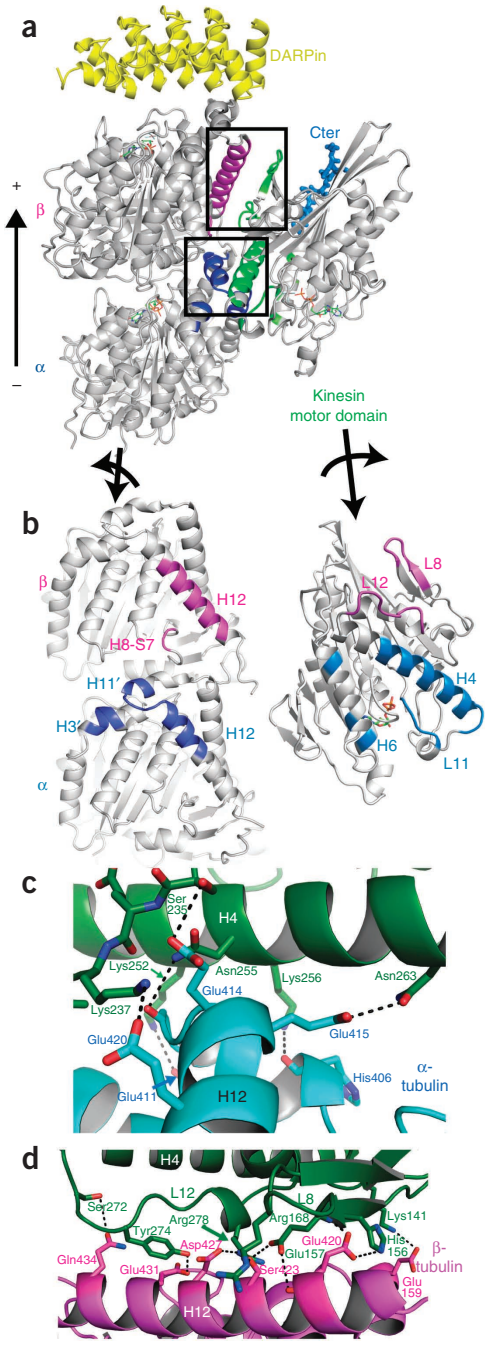

Figure 1 Structure of the tubulin–kinesin complex. (**a**) Overview of the complex crystallized. The arrow on the left indicates the direction of the axis and the polarity of a microtubule in which the tubulin has been incorporated. The kinesin neck linker is shown as a sticks model and is highlighted in blue. Contacting areas are colored blue and magenta on the α- and β-tubulin subunits, respectively, and green on the kinesin. Cter, C terminus. (**b**) The tubulin-kinesin interface. The contacting areas are colored as in **a** on tubulin (left). On kinesin (right), they are highlighted in colors corresponding to the subunit contacted. Secondary-structure elements in which the contacts are located are labeled according to established nomenclatures[26,35]. (**c**) The interface of the kinesin with α-tubulin. Here, as in **d**, only residues that establish a hydrogen bond or salt bridge with tubulin are displayed. (Additional detailed views of this interface are presented in **Fig. 3a** and **Supplementary Fig. 5b**.) (**d**) The interface of the kinesin with β-tubulin. (**Supplementary Fig. 5a** shows a detailed view centered on kinesin residue Arg278.) All figures were generated with PyMOL (http://www.pymol.org/). Hydrogen bonds, potential salt bridges and Mg^{2+} interactions are marked as dashed black lines throughout.

Table 2 Data collection and refinement statistics

	Tubulin–kinesin–ADP–AlF_4^-	
	Uncorrected for anisotropy	Corrected for anisotropy[a]
Data collection		
Space group	$P2_12_12_1$	$P2_12_12_1$
Cell dimensions		
a, *b*, *c* (Å)	77.05, 160.54, 174.95	77.05, 160.54, 174.95
Resolution (Å)	50–3.19 (3.27–3.19)[b]	50–3.19 (3.27–3.19)
R_{merge}	0.146 (1.717)	0.129 (0.476)
$I / \sigma I$	16.3 (1.71)	19.03 (4.56)
Completeness (%)	99.6 (95.9)	80.3 (21.4)
Redundancy	24.8 (9.96)	25.8 (6.6)
Refinement		
Resolution (Å)	3.19	3.19
No. reflections	36,892	29,641
R_{work} / R_{free}	0.169 / 0.208	0.178 / 0.212
No. atoms		
Protein	10,510	10,510
Ligand/ion	100	100
Water	2	2
B factors		
Protein	168	80.4
Ligand/ion	152	65.4
Water	146	63.2
r.m.s. deviations		
Bond lengths (Å)	0.010	0.010
Bond angles (°)	1.22	1.22

Five data sets collected from three crystals were merged together and processed as described in Online Methods.
[a]Coordinates deposited in the Protein Data Bank. [b]Values in parentheses are for the highest-resolution shell.

its H8–S7 loop and, on the kinesin side, by L8 and L12 and by the S5a β-strand inserted in L8 (**Fig. 1b**,**d**). The two zones were likely to contribute similarly to the interaction, as indicated by the respective buried surface areas and numbers of potential hydrogen bonds established: 630 Å^2 buried and six hydrogen bonds with α-tubulin compared to 540 Å^2 buried and eight hydrogen bonds with β-tubulin.

A prominent general feature of the complex is that tubulin is curved, similarly to its conformation in other nonmicrotubular structures[16,17] (**Supplementary Fig. 2**), whereas it is straight in microtubules[18] along which the kinesin moves. This raised questions regarding the similarity of kinesin structures when microtubule bound or in the complex we crystallized and regarding the similarity of the corresponding tubulin-kinesin interfaces. We have addressed these questions by comparing our structure to cryo-EM data on kinesin-1 bound to microtubules[9]. The structure of kinesin in its complex with tubulin docked well into the kinesin electron density derived from EM analysis of microtubules decorated with AMP-PNP–bound kinesin monomers (**Fig. 2a**). Because tubulin was curved in the complex we crystallized, once the kinesin motor domain was adjusted in the kinesin electron density of decorated microtubules, additional rotations were needed to adjust the α- and β-tubulin subunits to the microtubular electron density (**Fig. 2b**). Nevertheless, these rotations were small (7° and 2° for α- and β-tubulin, respectively), and, moreover, the deviations of the Cαs between tubulin residues at the tubulin-kinesin interface in the complex and the same residues in microtubules were limited (r.m.s. deviation 0.9 Å), close to the expected atomic-coordinate accuracy of the structure (0.66 Å, described in Online Methods). There were several reasons for this small deviation. First, the kinesin mostly interacted with the C-terminal helical hairpins of both tubulin subunits, regions that do not change conformation but rotate as a whole with their respective subunits upon tubulin's transition from curved to straight[19]. Second, α-tubulin residues that interacted with the kinesin were close to the axis of the rotation that adjusted this subunit in the microtubule electron density. Finally, β-tubulin residues at the kinesin interface moved very little because the angle of the rotation that fits this subunit was small (2°). As a result, among the 14 potential hydrogen bonds identified in the tubulin–kinesin complex, ten were still established in the fitted structure (**Supplementary Fig. 3a**,**b**), without any adjustment other than rigid body rotations. Moreover, because the tubulin-kinesin interaction was largely contributed to by residues in flexible loops (kinesin L8 and L12, α-tubulin H11′–H12 and β-tubulin H8–S7), it was likely that, following small adjustments of these loops or of flexible side chains, nearly all the interactions with curved tubulin would also be made in the physiological complex. This provided the basis for the identification of interactions that give rise to movement from the structure we determined.

Changes of kinesin in the complex and the ATPase mechanism

There were multiple local conformational changes to tubulin-bound kinesin–ATP compared to unbound kinesin–ADP. They included in particular an elongation of the H4 helix of the kinesin motor at its N terminus (**Fig. 3a**). This elongation was stabilized by interactions with α-tubulin and was seen in EM structures of decorated microtubules in all the kinesin nucleotide states[7–9]. The kinesin nucleotide also had specific effects on the conformation of its binding pocket. The ATP third phosphate (or its AlF_4^- analog) and the nucleotide-bound

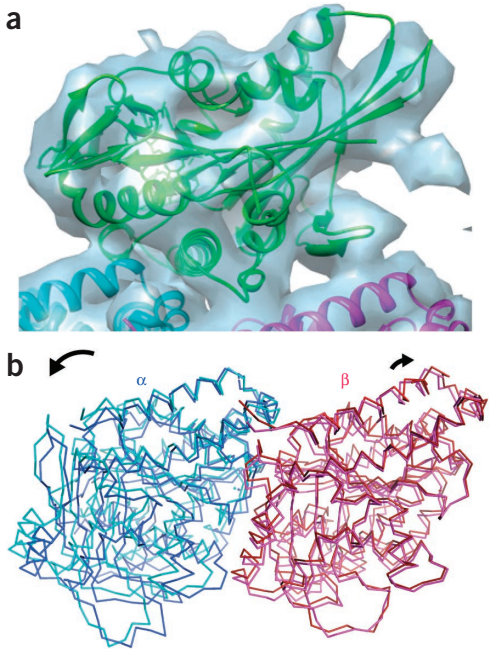

Figure 2 The adjustment of the proteins of the tubulin–kinesin complex in the cryo-EM envelope of kinesin-1–decorated microtubules. (**a**) The kinesin structure in the tubulin–kinesin complex docked in the cryo-EM volume of the kinesin from a previous structure of microtubules decorated with kinesin–AMP-PNP[9]. Docking was initially done manually and followed by rigid body fitting with UCSF Chimera[36], resulting in a 0.93 cross-correlation score between an 8-Å map simulated from the kinesin coordinates and the cryo-EM map[9]. (**b**) Comparison of the tubulin structures before and after subunit adjustment in the microtubule electron density. The sizes of the arrows reflect the amplitude of the rotations required for the adjustment.

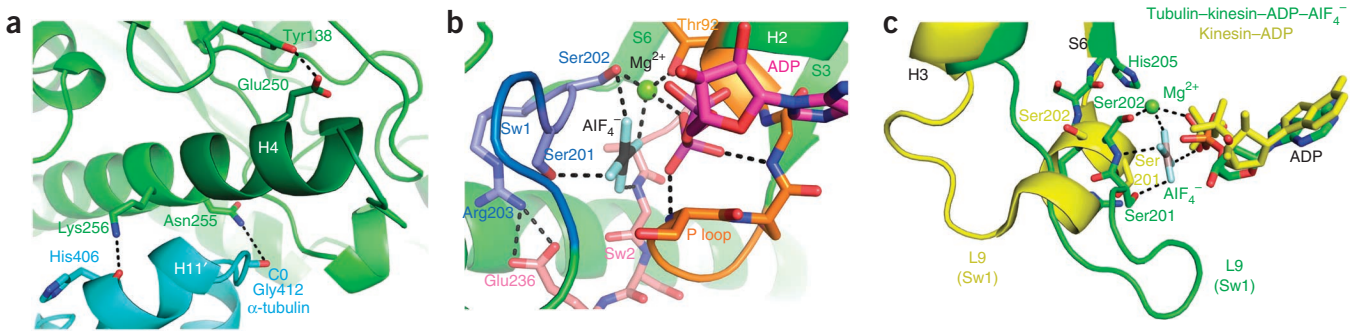

Figure 3 Conformational changes in tubulin-bound kinesin–ATP. (**a**) Structure of the H4 helix in tubulin-bound kinesin. Interactions with the kinesin motor domain (green) and with α-tubulin residues (cyan) are shown. H4 residues that are part of the extension in the tubulin-bound kinesin are in darker green. CO, carbonyl of Gly412. (**b**) Interactions of ADP–AlF_4^-–Mg^{2+} with the nucleotide-binding motifs (blue, Sw1; pink, Sw2; orange, P loop). (**c**) Conformational changes of L9. L9 in the tubulin–kinesin complex (this work, green) and in tubulin–unbound kinesin[11] (yellow) are compared after the central β-sheets of the two kinesin structures have been superimposed.

Mg^{2+} ion established several hydrogen bonds with three nucleotide-binding motifs (Switch1 (Sw1), Switch2 (Sw2) and the P loop) that are found in all kinesins, as in G proteins. These hydrogen bonds, made in particular with two universally conserved serine residues in Sw1 (**Fig. 3b**), led to a pronounced conformational change of L9, in which this motif is embedded (**Fig. 3c**). A hydrogen bond was also made with Sw2, which is embedded in L11 and underwent a marked conformational change as well (described below).

In kinesins, Sw1, Sw2 and the P loop completely define the environment of the nucleotide's phosphates[20] and therefore the ATPase mechanism. In many kinesins, in the absence of microtubules, variable, nucleotide-independent conformations of the nucleotide-binding loops are observed[21]. However, a few kinesins[22–24], including Eg5 (ref. 24; a kinesin-5), populate nucleotide-dependent conformational states when isolated. The conformations of the nucleotide-binding site in isolated Eg5–AMP-PNP and in the tubulin–kinesin complex were similar (**Fig. 4a**); therefore, they probably share the same ATPase mechanism. Because the Eg5–AMP-PNP structure was determined at a resolution (2.2 Å) that allows water molecules to be localized, this structure defines water molecules that are important for the mechanism of ATP hydrolysis by tubulin-bound kinesin. The mechanism proposed is base catalysis, with the general base being a water molecule that abstracts a proton from the water nucleophile[24]. The general-base water molecule is activated by the Sw2 C-terminal residue (Glu236 in kinesin-1), which relocated in kinesin–ATP upon tubulin binding. Two factors contributed to relocate Glu236: Sw2 was embedded in L11, which contacted tubulin and became ordered in the tubulin–kinesin complex (**Fig. 4b**), and Glu236 made a salt bridge with Sw1 residue Arg203 (**Figs. 3b** and **4**). Notably, both Glu236 and Arg203 are universally conserved in kinesins. The relocation of Glu236, which allowed it to activate the general base of the ATPase mechanism, accounted for the observation that the rate of the kinesin ATPase chemical step[10] was noticeably accelerated by tubulin (**Table 1**).

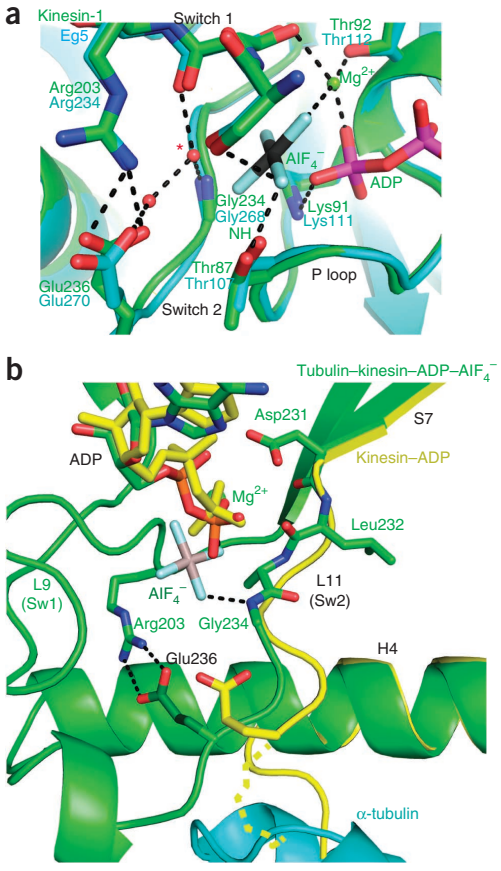

Figure 4 The kinesin-1 and Eg5 ATP-binding sites superpose well. (**a**) Residues important for catalysis in Eg5 (ref. 24; cyan) and the corresponding kinesin-1 residues in the tubulin–kinesin complex (green), shown following superposition of the two motor domains (r.m.s. deviation of Cα positions of 0.635 Å for 256 atoms superimposed out of 322). The two water molecules presented (red spheres) are particularly important for catalysis in Eg5 (ref. 24); the one involved in the nucleophilic attack of the ATP γ-phosphate is marked by an asterisk. The kinesin-1 nucleotide (ADP–AlF_4^-) is the only one displayed. (**b**) Comparison of L11 in tubulin–kinesin (this work, green) and in tubulin–unbound kinesin[11] (yellow). This comparison is made after the central β-sheets of the two kinesin structures have been superimposed. In free kinesin-1, the Lys237–Ala251 part of L11 that is poorly defined or not defined is drawn as a dashed line.

The mechanism for neck-linker docking in a motile kinesin

In tubulin–kinesin–ADP–AlF_4^-, the neck linker was docked on the catalytic core of the motor domain. Its first residue, Ile325, immediately C terminal to H6 and largely conserved in kinesins, was buried in a hydrophobic pocket in the core of the motor domain, as in structures of tubulin-free kinesins with docked neck linker[11,24,25]. The walls of this pocket were made by the side chains of consensus

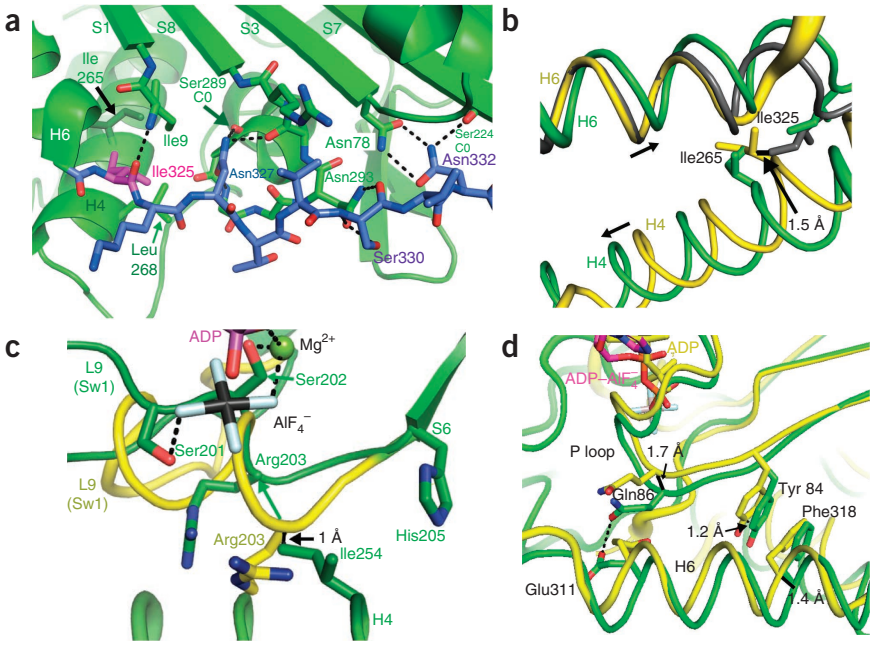

Figure 5 Neck-linker docking in tubulin-bound kinesin–ADP–AlF_4^-. (**a**) Interactions of the neck linker (blue) with the catalytic core (green). Eight residues at the N-terminal end of the kinesin have been omitted for clarity. (**b**) Positions of H4 and H6 in the kinesin motor with neck linker docked and undocked. Here, as in **c** and **d**, kinesin–ADP (undocked[26], yellow) and tubulin-bound kinesin–ADP–AlF_4^- (docked, this work, green) are compared after the motor domain β-sheets have been superimposed. Black arrows indicate the opposite directions of H4 and H6 translations. In unbound kinesin, helix H6 has been extended by one turn (gray), modeled to show the position Ile325 would adopt if the helix had not unwound and the resulting clash with H4 residue Ile265. (**c**) The Sw1 conformational change in tubulin-bound kinesin–ADP–AlF_4^-. Sw1 in kinesin–ADP is displayed together with H4 and Sw1 in tubulin–kinesin–ADP–AlF_4^-. The clash of Ile254 side chain from the latter complex with Arg203 Cα in kinesin–ADP is highlighted as a black solid line. The green arrow shows the change of Arg203 location that avoids this clash. (**d**) The P-loop conformational change. H6 and the P loop are displayed in kinesin–ADP and tubulin–kinesin–ADP–AlF_4^- together with the nucleotide.

kinesin residues in H4 (Ile265 and Leu268) and at the N-terminal end of the protein (Ile9). Additional stabilization of the neck linker came from hydrogen bonds between four of its first eight residues and the catalytic core; two of these residues (Asn327 and Asn332) are universally conserved[12] (**Fig. 5a**).

The structural rationale for the docking of the neck linker was clearly revealed by a comparison of the tubulin-bound kinesin structure (this work) with one in which the neck linker is undocked[26]. Superposition of the central β-sheet of the two kinesins (r.m.s. deviation 0.4 Å, 58 Cαs superimposed) showed that neck-linker docking was accompanied by translations of H6 and H4 (by 1.4 Å and 2.6 Å, respectively) (**Fig. 5b**). There was also a small (7°) H4 rotation, but its contribution to the movement of the helix was minor (one one-fifth of the total). In the undocked kinesin, if the neck linker was modeled to dock as in the complex, a clash occurred between Ile325 and the consensus H4 residue Ile265 (**Fig. 5b**). This clash is avoided as the last turn of helix H6 unwinds, thus resulting in neck-linker undocking. Therefore, neck-linker docking requires the translations of H4 and H6. The question that arises then is how H4 and H6 translations are favored in tubulin- or microtubule-bound kinesin–ATP.

When the kinesin was bound to microtubules[7,9] or to tubulin, H4 was elongated at its N-terminal end (**Fig. 3a**). Interactions with tubulin that induced it to elongate also contributed to determination of its location in the complex. As a result, the strictly conserved H4 residue Ile254 would have severely clashed with Arg203 (in Sw1) if Sw1 had the conformation that it adopts in kinesin–ADP[26] (**Fig. 5c**). In the complex, the Sw1 main chain was displaced (**Fig. 3c**) because of its interactions with the nucleotide and with Sw2 (**Fig. 3b**), thus allowing for Ile254 to be accommodated (**Fig. 5c**) and for H4 to occupy its translated location. The Sw1 conformational change was accompanied by a nucleotide displacement, as compared to the structure of free kinesin–ADP (**Fig. 3c**), favoring in turn a P-loop movement (**Supplementary Fig. 4**) and an ~1-Å translation of the Tyr84 side chain (**Fig. 5d**). Tyr84, a conserved residue specific to the kinesin P loop[27], was in a stacking interaction with the H6 consensus residue Phe318. Consequently, the P-loop movement pushed H6 in a direction almost parallel to its axis, toward its C-terminal end. In conclusion, the translations of H4 and H6 in kinesin were induced by binding of tubulin and ATP, respectively, which explained why neck-linker docking is allowed in microtubule-bound kinesin–ATP. As the interactions of the neck linker with the core of the motor domain then favored its docked conformation, the neck linker was predominantly docked in microtubule-bound kinesin–ATP. Taken together, our data defined integrated connections between the nucleotide-binding pocket and the neck linker, two sites that are >20 Å apart. These connections participate in establishing a relationship between neck docking and the nucleotide state of microtubule-bound kinesin, which is crucial for the transportation of loads by kinesins moving along microtubules.

DISCUSSION

In this study, we have determined the structure of the complex of a motile kinesin-1 monomeric functional domain with tubulin. This structure represented a power stroke–generating conformation of microtubule-bound kinesin and defined the binding interface between kinesin and tubulin. Some of the critical residues at the interface have been identified previously in an extensive alanine scan of kinesin surface residues[28]. Their mutations that weaken kinesin binding to microtubules lead to increases in K_m of microtubule-stimulated ATPase. For instance, the most severely affected mutant, R278A, has a K_m increased by more than an order of magnitude. Indeed, Arg278 is located in the tubulin-interacting L12 and interacts with Asp427 in the mostly acidic exposed face of β-tubulin helix H12 (**Supplementary Fig. 5a**). Notably, several of the acidic exposed residues of this helix are associated with tubulin dominant mutations involved in neurological disorders and impair kinesin interactions with microtubules[29,30]. The tubulin–kinesin structure therefore explained changes in the interaction with microtubules of *in vitro*–generated kinesin mutants and provided a rationale for the involvement of kinesins in the phenotypes of some disease-causing tubulin mutants.

Our results have also allowed us to address open questions regarding the generation of movement by kinesins. One of them concerns

the mechanism by which binding of the motile kinesin motor to microtubules markedly accelerates its ATPase activity. ATP hydrolysis is required for movement because it prevents a kinesin from being stalled on a microtubule[31]. The ATP turnover cycle of isolated kinesin-1 is limited by ADP release, which is considerably accelerated by microtubules[32]. In addition, microtubules enhance the rate constant of the chemical step[10]. The chemical step is initiated in the complex of microtubule-bound kinesin–ATP, which is trapped when the nucleotide is replaced by its nonhydrolyzable analog AMP-PNP. We have seen that the active site of kinesin-1 bound to tubulin and to ADP–AlF_4^- superimposed well with that of isolated Eg5 bound to AMP-PNP (**Fig. 4a**). The same holds true with the active site of an isolated kinesin-4–AMP-PNP[22]. These results suggested that the ATPase mechanism proposed on the basis of the high-resolution Eg5–AMP-PNP structure, despite the absence of bound tubulin, was shared by tubulin-bound kinesin-1 and other motile kinesins. Because the interactions with ATP of the kinesin bound to tubulin or to microtubules were much alike (**Table 1**), the same ATPase mechanism (general, water mediated, base catalysis)[24] was likely to operate in both cases. Notably, the structure we determined also showed that tubulin or microtubules accelerated the chemical step of ATP hydrolysis by kinesins by stabilizing two interdependent conformational changes of L11 and L9 that brought into place the glutamate residue that indirectly activated the catalytic water nucleophile.

A second question concerns the structural changes of kinesin, elicited as it interacts with microtubules and binds ATP. Neck-linker docking was made possible by translational sliding of H4 and H6 with respect to the rest of the motor domain. It is therefore expected that mutations that interfere with the positioning of these two helices would impair motility and reduce velocity in a microtubule gliding assay. Indeed, in the same alanine scan of kinesin surface residues in which mutations that increase the K_m of microtubule-stimulated ATPase were identified, four mutations markedly decreased the microtubule gliding velocity[28]. Two of them are at residues Tyr138 and Glu250. Glu250 was close to the N-terminal end of H4 in tubulin-bound kinesin and made a hydrogen bond with Tyr138, the C-terminal residue of β-strand S4, in the core of the motor domain (**Fig. 3a**). This interaction therefore contributed to determination of the H4 position. The third mutation found, D140A, is positioned close to Tyr138; it is possible that this mutation changed the local structure of the kinesin and that its effect was indirect. The fourth mutation, Glu311, is at the N-terminal residue of helix H6, Glu311, which interacted with the nucleotide-binding loops: Glu311 made a hydrogen bond with Gln86 (in the P loop) (**Fig. 5d**) and made salt bridges with two conserved L11 residues, Lys237 (immediately C terminal to Sw2) and Lys240 (**Supplementary Fig. 5b**). These interactions favored the translated position of H6 and therefore neck-linker docking, leading to the prediction that Glu311 is important for kinesin motility as well as for its microtubule-stimulated ATPase activity. In a microtubule gliding assay, the velocity of the E311A mutant is one-third that of the wild-type protein, and its microtubule-stimulated ATPase rate[28] is reduced as well. The location in tubulin–kinesin of the mutants that affect microtubule gliding velocity and the interactions of the corresponding residues were consistent with the structural mechanism we proposed for neck-linker docking. This suggested that neck-linker docking is a crucial component in the changes that lead to the movement generated by kinesins.

The last question concerns the relation between the mechanisms to generate movement and force in kinesin-1 and in the evolutionarily related myosin. In myosin, force is produced during inorganic-phosphate release. In nucleotide-free rigor-like myosin, a substantial rearrangement of the core β-sheet of the upper 50-kDa subdomain results in a pronounced deviation compared to the nucleotide-bound structure[33,34] (r.m.s. deviation 0.93 Å, 47 Cαs superimposed, with the largest deviation (~4 Å) at the C-terminal end of the edge strand proximal to the one immediately following Sw1 in the sequence). This rearrangement causes ADP and inorganic-phosphate release and leads to a state in which force is produced, with the driving force for the power stroke being the transition from a low-affinity myosin–actin filament complex to a high-affinity one. In contrast with myosin, the β-sheet of tubulin-bound kinesin–ATP was twisted similarly to that in free kinesin–ADP (r.m.s. deviation 0.4 Å, 58 Cαs superimposed). This is also likely to be the case on the microtubule because the interfaces are highly similar (**Fig. 2**) and the kinesin–AMP-PNP dissociation constants from tubulin and microtubules are nearly identical (**Supplementary Table 1**). In the tubulin–kinesin–ATP-like complex, the neck linker established hydrogen bonds and hydrophobic interactions with the core of the motor domain (**Fig. 5a**). As they hold the neck linker in an orientation corresponding to the direction of the plus end of the microtubule (**Fig. 1a**), these interactions seem sufficient to bias binding of the second head in the direction of the movement. It is possible that, as with myosins, a strong interaction with microtubules, in that case of the second kinesin head, contributes to force production. Notably, the largest distortion of the kinesin central β-sheet in tubulin-bound kinesin–ATP (Cα deviation 1.2 Å) was at a location corresponding to that of the largest distortion in nucleotide-free myosin, a result raising the possibility that we witnessed the remnant of a much larger twist that only exists in the kinesin's rigor state. The structure of nucleotide-free kinesin complexed to tubulin will be required to establish whether, as within myosins, a pronounced distortion of the motor-domain central β-sheet accompanies nucleotide release. This will also establish how the neck linker is prevented from docking onto the core of the motor domain in the rigor state.

METHODS

Methods and any associated references are available in the online version of the paper.

Accession code. Coordinates and structure factors for the tubulin–kinesin–ADP–AlF_4^- X-ray structure have been deposited in the Protein Data Bank under accession code 4HNA.

Note: Supplementary information is available in the online version of the paper.

ACKNOWLEDGMENTS

We are grateful to J. Skehel and L. Amos for comments on the manuscript. We thank I. Mignot for assistance and D. Mauchand (Unité Commune d'Expérimentation Animale, Institut National de la Recherche Agronomique, Jouy en Josas, France) for providing us with the material from which tubulin was purified. We also thank R. Vale (University of California, San Francisco, San Francisco, California, USA) for giving us the kinesin plasmid. Diffraction data were collected at the European Synchrotron Research Facility (ID29) and at SOLEIL synchrotron (PX1). We thank the machine and beamline groups for making these experiments possible. This work has also benefited from the facilities and expertise of IMAGIF (Centre de Recherche de Gif). We gratefully acknowledge support by the French Fondation pour la Recherche Médicale (DEQ20081213979 to M.K.), Fondation ARC pour la Recherche sur le Cancer (to B.G.) and Agence Nationale de la Recherche (grants ANR-09-BLAN-0071 and ANR-12-BSV8-0002-01 to B.G.) and the Chinese Ministry of Education (grant NCET-10-0604 to C.W.) and Science and Technology Commission of Shanghai Municipality (grant 11JC1413100 to C.W.).

AUTHOR CONTRIBUTIONS

B.G., C.W. and M.K. designed research; B.G. crystallized the tubulin–DARPin–kinesin complex and determined its structure; W.W. and Q.J. characterized

the kinesin-tubulin interaction biochemically; L.P., B.D. and A.P. provided the DARPin; B.G., C.W. and M.K. analyzed the data; B.G., C.W. and M.K. wrote the manuscript with input from all other authors.

COMPETING FINANCIAL INTERESTS

The authors declare no competing financial interests.

Reprints and permissions information is available online at http://www.nature.com/reprints/index.html.

1. Hirokawa, N., Noda, Y., Tanaka, Y. & Niwa, S. Kinesin superfamily motor proteins and intracellular transport. *Nat. Rev. Mol. Cell Biol.* **10**, 682–696 (2009).
2. Wordeman, L. How kinesin motor proteins drive mitotic spindle function: lessons from molecular assays. *Semin. Cell Dev. Biol.* **21**, 260–268 (2010).
3. Lawrence, C.J. *et al.* A standardized kinesin nomenclature. *J. Cell Biol.* **167**, 19–22 (2004).
4. Howard, J. *Mechanics of Motor Proteins and the Cytoskeleton* (Sinauer, 2001).
5. Rice, S. *et al.* A structural change in the kinesin motor protein that drives motility. *Nature* **402**, 778–784 (1999).
6. Marx, A., Hoenger, A. & Mandelkow, E. Structures of kinesin motor proteins. *Cell Motil. Cytoskeleton* **66**, 958–966 (2009).
7. Hirose, K., Akimaru, E., Akiba, T., Endow, S.A. & Amos, L.A. Large conformational changes in a kinesin motor catalyzed by interaction with microtubules. *Mol. Cell* **23**, 913–923 (2006).
8. Kikkawa, M. & Hirokawa, N. High-resolution cryo-EM maps show the nucleotide binding pocket of KIF1A in open and closed conformations. *EMBO J.* **25**, 4187–4194 (2006).
9. Sindelar, C.V. & Downing, K.H. An atomic-level mechanism for activation of the kinesin molecular motors. *Proc. Natl. Acad. Sci. USA* **107**, 4111–4116 (2010).
10. Ma, Y.Z. & Taylor, E.W. Kinetic mechanism of a monomeric kinesin construct. *J. Biol. Chem.* **272**, 717–723 (1997).
11. Sindelar, C.V. *et al.* Two conformations in the human kinesin power stroke defined by X-ray crystallography and EPR spectroscopy. *Nat. Struct. Biol.* **9**, 844–848 (2002).
12. Vale, R.D. & Fletterick, R.J. The design plan of kinesin motors. *Annu. Rev. Cell Dev. Biol.* **13**, 745–777 (1997).
13. Yang, J.T., Saxton, W.M., Stewart, R.J., Raff, E.C. & Goldstein, L.S. Evidence that the head of kinesin is sufficient for force generation and motility *in vitro*. *Science* **249**, 42–47 (1990).
14. Alonso, M.C. *et al.* An ATP gate controls tubulin binding by the tethered head of kinesin-1. *Science* **316**, 120–123 (2007).
15. Amos, L.A. & Hirose, K. The structure of microtubule–motor complexes. *Curr. Opin. Cell Biol.* **9**, 4–11 (1997).
16. Mignot, I. *et al.* Design and characterization of modular scaffolds for tubulin assembly. *J. Biol. Chem.* **287**, 31085–31094 (2012).
17. Pecqueur, L. *et al.* A designed ankyrin repeat protein selected to bind to tubulin caps the microtubule plus end. *Proc. Natl. Acad. Sci. USA* **109**, 12011–12016 (2012).
18. Nogales, E., Whittaker, M., Milligan, R.A. & Downing, K.H. High-resolution model of the microtubule. *Cell* **96**, 79–88 (1999).
19. Ravelli, R.B. *et al.* Insight into tubulin regulation from a complex with colchicine and a stathmin-like domain. *Nature* **428**, 198–202 (2004).
20. Sack, S., Kull, F.J. & Mandelkow, E. Motor proteins of the kinesin family: structures, variations, and nucleotide binding sites. *Eur. J. Biochem.* **262**, 1–11 (1999).
21. Grant, B.J., McCammon, J.A., Caves, L.S. & Cross, R.A. Multivariate analysis of conserved sequence-structure relationships in kinesins: coupling of the active site and a tubulin-binding sub-domain. *J. Mol. Biol.* **368**, 1231–1248 (2007).
22. Chang, Q., Nitta, R., Inoue, S. & Hirokawa, N. Structural basis for the ATP-induced isomerization of kinesin. *J. Mol. Biol.* **425**, 1869–1880 (2013).
23. Kikkawa, M. *et al.* Switch-based mechanism of kinesin motors. *Nature* **411**, 439–445 (2001).
24. Parke, C.L., Wojcik, E.J., Kim, S. & Worthylake, D.K. ATP hydrolysis in Eg5 kinesin involves a catalytic two-water mechanism. *J. Biol. Chem.* **285**, 5859–5867 (2010).
25. Sack, S. *et al.* X-ray structure of motor and neck domains from rat brain kinesin. *Biochemistry* **36**, 16155–16165 (1997).
26. Kull, F.J., Sablin, E.P., Lau, R., Fletterick, R.J. & Vale, R.D. Crystal structure of the kinesin motor domain reveals a structural similarity to myosin. *Nature* **380**, 550–555 (1996).
27. Leipe, D.D., Wolf, Y.I., Koonin, E.V. & Aravind, L. Classification and evolution of P-loop GTPases and related ATPases. *J. Mol. Biol.* **317**, 41–72 (2002).
28. Woehlke, G. *et al.* Microtubule interaction site of the kinesin motor. *Cell* **90**, 207–216 (1997).
29. Cederquist, G.Y. *et al.* An inherited TUBB2B mutation alters a kinesin-binding site and causes polymicrogyria, CFEOM and axon dysinnervation. *Hum. Mol. Genet.* **21**, 5484–5499 (2012).
30. Tischfield, M.A. *et al.* Human TUBB3 mutations perturb microtubule dynamics, kinesin interactions, and axon guidance. *Cell* **140**, 74–87 (2010).
31. Cross, R.A. The kinetic mechanism of kinesin. *Trends Biochem. Sci.* **29**, 301–309 (2004).
32. Hackney, D.D. Kinesin ATPase: rate-limiting ADP release. *Proc. Natl. Acad. Sci. USA* **85**, 6314–6318 (1988).
33. Coureux, P.D. *et al.* A structural state of the myosin V motor without bound nucleotide. *Nature* **425**, 419–423 (2003).
34. Reubold, T.F., Eschenburg, S., Becker, A., Kull, F.J. & Manstein, D.J. A structural model for actin-induced nucleotide release in myosin. *Nat. Struct. Biol.* **10**, 826–830 (2003).
35. Löwe, J., Li, H., Downing, K.H. & Nogales, E. Refined structure of αβ-tubulin at 3.5 Å resolution. *J. Mol. Biol.* **313**, 1045–1057 (2001).
36. Pettersen, E.F. *et al.* UCSF Chimera: a visualization system for exploratory research and analysis. *J. Comput. Chem.* **25**, 1605–1612 (2004).

ONLINE METHODS

Proteins. Tubulin was purified from ovine brain as described[37]. Before use, a cycle of microtubule assembly-disassembly was performed to remove any non-functional protein. A designed ankyrin repeat protein[38] (DARPin) was used to stabilize tubulin and to crystallize tubulin-kinesin. It was selected in a screen for tubulin binding and inhibition of microtubule assembly[17] and produced as described[16,17]. A cys-light version of a monomeric construct of human kinesin-1 (ref. 5) (residues 1–349, kind gift of R. Vale) was expressed in *E. coli*, purified in two steps by anion-exchange chromatography and stored in liquid nitrogen until use. For affinity measurement with fluorescence anisotropy, an S188C mutation was introduced for protein labeling[39]. This mutation did not change the kinesin ATPase activity (Q.J., unpublished data). Taxotere-stabilized microtubules were used for binding affinity and ATPase-stimulation measurements.

ATPase and affinity measurements. The ATPase activities of kinesin-1 were measured at 25 °C with an enzyme-coupled assay, as described[40], in a buffer consisting of 20 mM PIPES, pH 6.8, 1 mM $MgCl_2$, 0.5 mM EGTA, 1 mM DTT and 1 mM ATP. For microtubule-stimulated ATPase activity measurement, 20 μM Taxotere was supplemented in the buffer to stabilize microtubules. For binding-affinity measurements, monomeric kinesin-1 with the S188C mutation was labeled with fluorescein-5-maleimide. The binding between kinesin and tubulin or microtubules was measured by monitoring the anisotropy of labeled kinesin-1 fluorescence in 20 mM PIPES, pH 6.8, 1 mM $MgCl_2$ and 0.5 mM EGTA supplemented with either 1 mM ADP, 1 mM AMP-PNP or 1 mM ADP with 2 mM $AlCl_3$ and 10 mM KF to mimic the transition state of ATP hydrolysis. The dissociation constant was calculated as described[40].

Complex preparation and crystallization. For preparation of the complex with kinesin in the AMP-PNP state, monomeric kinesin-1 was first desalted through a Micro Bio-Spin column (Bio-Rad) to remove unbound nucleotide. It was then incubated in the presence of 1 mM AMP-PNP with the tubulin–DARPin complex. After a 40-min incubation on ice, the mixture was desalted through a PD10 column (GE healthcare) equilibrated with 15 mM PIPES-K, pH 6.8, 0.5 mM $MgCl_2$, 0.4 mM EGTA and 0.1 mM GDP. AMP-PNP (0.5 mM) was added right afterward to the protein-containing fractions. The complex was concentrated to an A_{278} of ~20. Crystals were obtained at pH 6.8 with polyethylene glycol (PEG) 20000 as precipitant. For the structure with kinesin in the ADP–AlF_4^- state (and β-tubulin in GDP–AlF_4^-), the complex was prepared essentially in the same way. Purified monomeric kinesin desalted with a microbiospin device was incubated with tubulin–DARPin before a desalting step on PD10 was performed as above. The complex-containing fractions, in which the kinesin was essentially nucleotide-free, were concentrated to reach an A_{278} of ~35. Just before crystallization, the complex was supplemented with 1 mM ADP and crystallized by vapor diffusion at 293 K in 8–10% (w/v) PEG 20000, 30 mM PIPES-K, pH 6.8, 0.8 mM $AlCl_3$ and 4 mM NaF. Crystals were transferred in a buffer consisting of 9% PEG 20000, 30 mM PIPES, 1 mM $MgCl_2$, 0.1 mM GDP, 0.5 mM ADP, 1 mM $AlCl_3$, 5 mM NaF and 25% glycerol before being flash cooled in liquid nitrogen.

Data collection, structure solution and refinement. Preliminary diffraction experiments were performed at the Proxima1 beamline (SOLEIL synchrotron, Saint Aubin, France). Complete data sets were collected at 100 K at the ID29 beamline (European Synchrotron Radiation Facility, Grenoble, France). The crystals belong to the $P2_12_12_1$ space group, and there is one complex per asymmetric unit. The diffraction is highly anisotropic, with a limit close to 3 Å along the b* and c* axis but <4 Å along the a* axis. To compensate to some extent for anisotropy, five data sets collected from three crystals were merged. The data sets were processed with XDS[41], after which two strategies were used in parallel: data were either merged with XSCALE, then scaled, reduced and corrected for anisotropy with a previously described method[42] available at http://services.mbi.ucla.edu/anisoscale/ (corrected data), or they were scaled and merged with XSCALE[43] (uncorrected data). Data processing statistics for both strategies are given in **Table 2**. The structure was solved by molecular replacement with Amore[44]. The models used were PDB 1BG2 (ref. 26), in which L11 was removed for the kinesin, and PDB 3RYC (ref. 45) for tubulin. After the tubulin and the kinesin had been placed and rigid body refined, a molecular replacement solution was found for the DARPin, which completed the initial model. The structures were refined with Buster (http://www.globalphasing.com/buster/), alternating refinement with model building in Coot[46]. For the crystals obtained in the presence of ADP, $AlCl_3$ and NaF, additional signals in the nucleotide-binding sites of the kinesin (**Supplementary Fig. 1**) and of the tubulin β subunit were attributed to AlF_4^-. Constraints were applied during refinement to keep standard bond distances between AlF_4^-, nucleotide, Mg^{2+} and protein-coordinated atoms. In the kinesin nucleotide-binding site, two water molecules were modeled with the Eg5–AMP-PNP structure as a reference[24] (PDB 3HQD) for Mg^{2+} to be hexacoordinated (**Supplementary Fig. 1**).

Most calculations were performed with the data corrected for anisotropy. Some refinement cycles were performed in parallel with data originating from both procedures; they led to essentially the same model. As an example, the r.m.s. deviation after superposition of the 1,350 Cαs of the final models is 0.04 Å. The Ramachandran statistics are also similar: for the model refined against the corrected data, 95.7% and 3.4% of the residues are in the favored and allowed regions of the Ramachandran plots, respectively, and 0.9% are outliers, as evaluated with MolProbity[47]. The corresponding values for the model refined against the uncorrected data set are 96.2%, 3.05% and 0.75%. Finally, the refinement statistics are also close, but with much higher *B* factors for uncorrected data (**Table 2**) and a corresponding lower precision of atomic coordinates (errors are 1.17 Å and 0.66 Å for uncorrected and corrected data, respectively, as estimated from Luzzati plots). The electron density maps are also much improved after anisotropy correction (**Supplementary Fig. 6**). Coordinates originating from refinement against the corrected data together with structure factors both corrected for anisotropy and uncorrected have been deposited in the Protein Data Bank (PDB 4HNA). The final model does not include residues 39–45 and the C terminus starting from residue 438 for the tubulin α subunit, the C terminus starting from residue 442 for β, the ten N-terminal residues of the DARPin (that is, the His tag) and the four N-terminal residues and the C terminus starting from residue 338 for kinesin.

37. Castoldi, M. & Popov, A.V. Purification of brain tubulin through two cycles of polymerization-depolymerization in a high-molarity buffer. *Protein Expr. Purif.* **32**, 83–88 (2003).
38. Binz, H.K. *et al.* High-affinity binders selected from designed ankyrin repeat protein libraries. *Nat. Biotechnol.* **22**, 575–582 (2004).
39. Wong, Y.L. & Rice, S.E. Kinesin's light chains inhibit the head- and microtubule-binding activity of its tail. *Proc. Natl. Acad. Sci. USA* **107**, 11781–11786 (2010).
40. Wang, W. *et al.* Kif2C minimal functional domain has unusual nucleotide binding properties that are adapted to microtubule depolymerization. *J. Biol. Chem.* **287**, 15143–15153 (2012).
41. Kabsch, W. Xds. *Acta Crystallogr. D Biol. Crystallogr.* **66**, 125–132 (2010).
42. Strong, M. *et al.* Toward the structural genomics of complexes: crystal structure of a PE/PPE protein complex from *Mycobacterium tuberculosis*. *Proc. Natl. Acad. Sci. USA* **103**, 8060–8065 (2006).
43. Kabsch, W. Integration, scaling, space-group assignment and post-refinement. *Acta Crystallogr. D Biol. Crystallogr.* **66**, 133–144 (2010).
44. Navaza, J. AMoRe: an automated package for molecular replacement. *Acta Crystallogr. A* **50**, 157–163 (1994).
45. Nawrotek, A., Knossow, M. & Gigant, B. The determinants that govern microtubule assembly from the atomic structure of GTP-tubulin. *J. Mol. Biol.* **412**, 35–42 (2011).
46. Emsley, P., Lohkamp, B., Scott, W.G. & Cowtan, K. Features and development of Coot. *Acta Crystallogr. D Biol. Crystallogr.* **66**, 486–501 (2010).
47. Chen, V.B. *et al.* MolProbity: all-atom structure validation for macromolecular crystallography. *Acta Crystallogr. D Biol. Crystallogr.* **66**, 12–21 (2010).